**Supporting Information**

# Regulating the electronic and spin structure of endohedral metallofullerene: A case investigation on $Sc_3N@C_{80}$ and $Sc_3C_2@C_{80}$

Yongqiang Feng,*[a] Yuzhu Hu,[a] Tianmi Luo,[a] Chengke Yuan,[a] Wenjie Zhu,[a] Mengting Gao[a] and Xuemeng Huo[a]

[a] School of Materials Science and Engineering, Shaanxi Key Laboratory of Green Preparation and Functionalization for Inorganic Materials, Shaanxi University of Science and Technology, Xi'an, 710021, China

* Correspondence: fengyq@sust.edu.cn

## Additional Figures

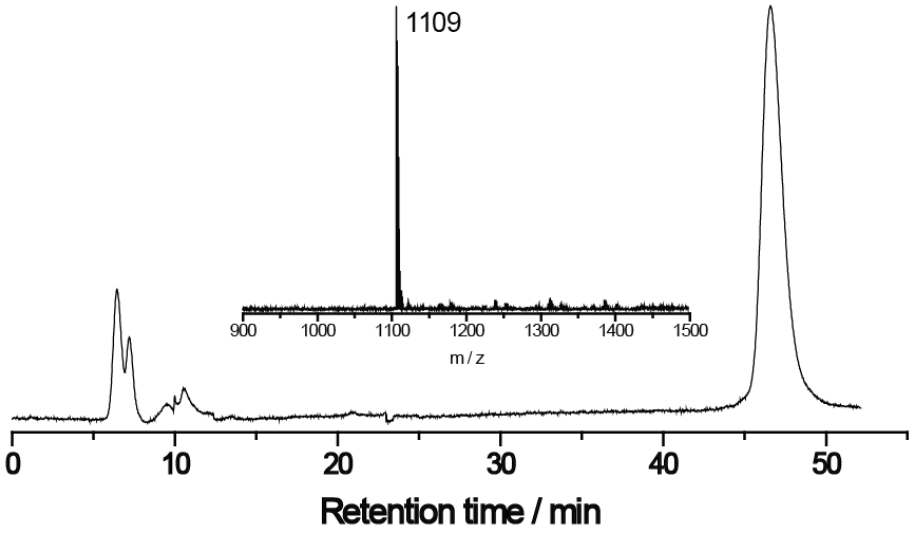


Figure S1. HPLC profile of the purified $Sc_3N@C_{80}$. Conditions: Buckyprep column (ø 20 mm × 250 mm), 12 mL $min^{-1}$ toluene flow, 310 nm detection wavelength. Inset: MALDI-TOF mass spectroscopy of $Sc_3N@C_{80}$.

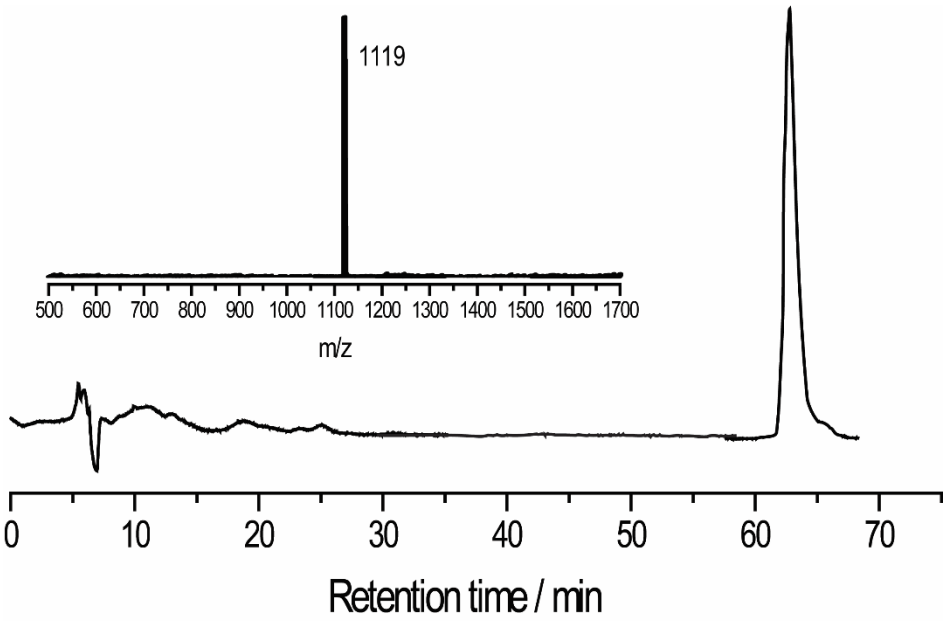


Figure S2. HPLC profile of the purified $Sc_3C_2@C_{80}$. Conditions: Buckyprep column (ø 20×250 mm), 12 mL $min^{-1}$ toluene flow, 310 nm detection wavelength. Inset: MALDI-TOF mass spectroscopy of $Sc_3C_2@C_{80}$.

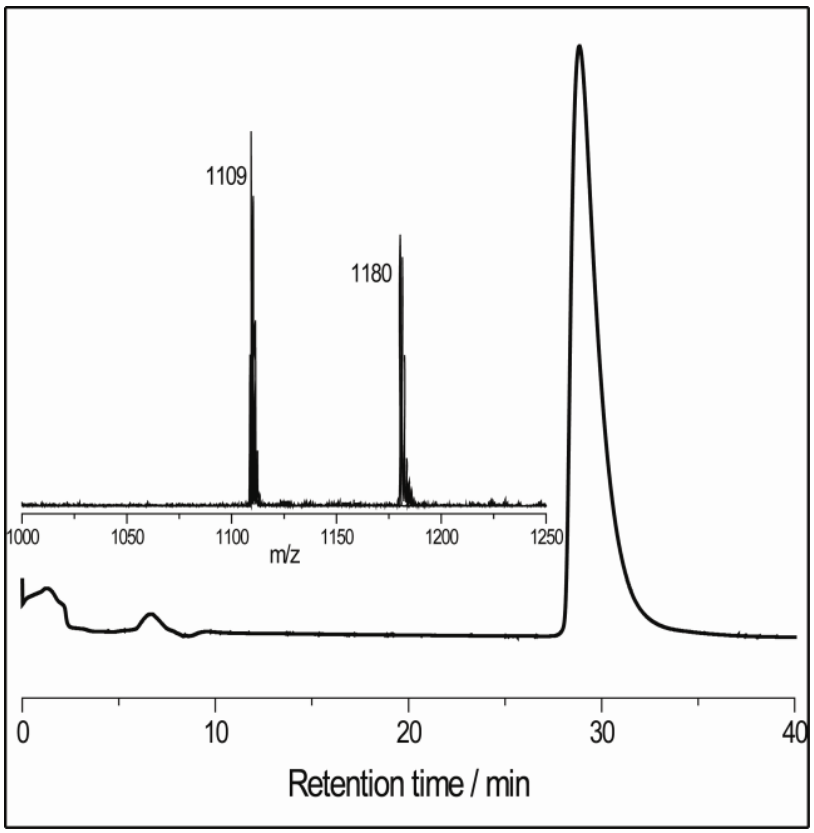


Figure S3. HPLC profile of monoadduct of $Sc_3N@C_{80}$-Gly. Conditions: Buckyprep-M column (ø 20×250 mm), 12 mL $min^{-1}$ toluene flow, 310 nm detection wavelength. Inset: MALDI-TOF mass spectroscopy of $Sc_3N@C_{80}$-Gly.

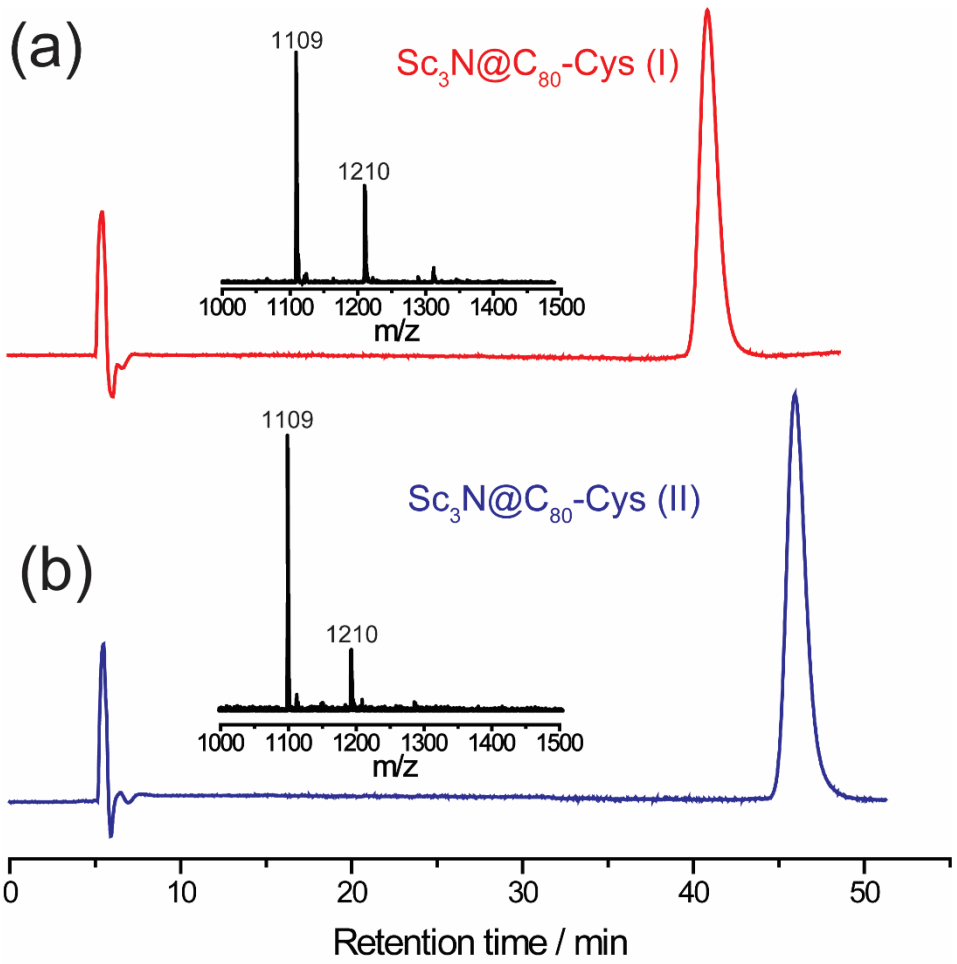


Figure S4. HPLC profiles of purified (a) $Sc_3N@C_{80}$-Cys (I) and (b) $Sc_3N@C_{80}$-Cys (II), inset showing the corresponding MALDI-TOF-MS data.

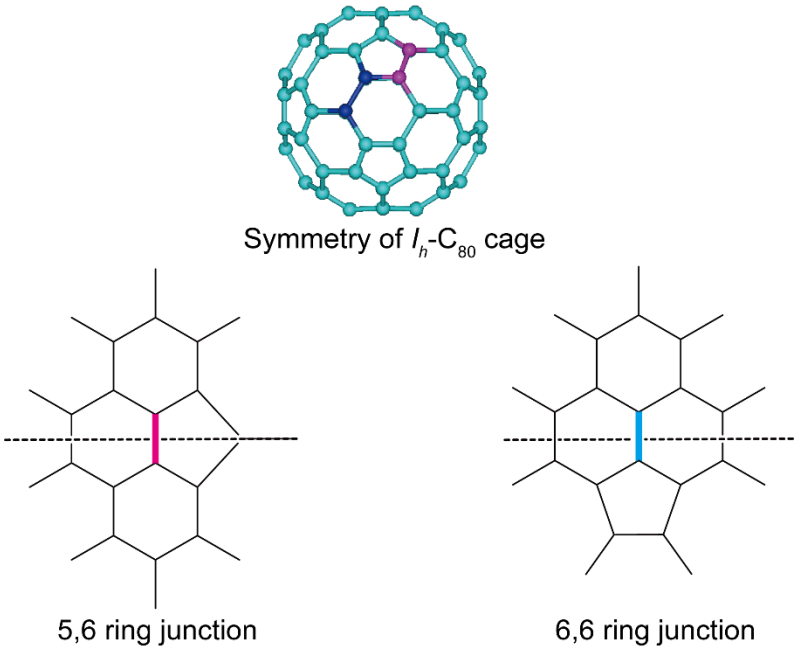


Figure S5. Two addition sites on the $I_h$-$C_{80}$ carbon cage.

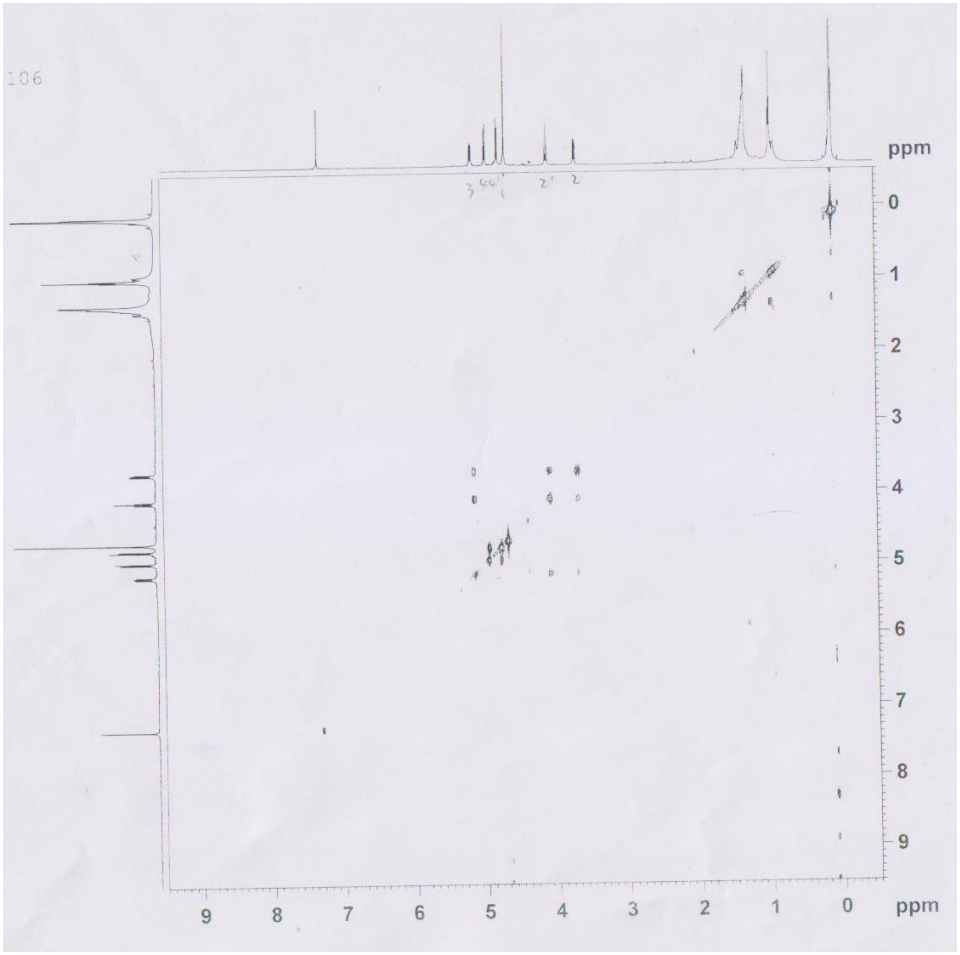


Figure S6. COSY spectrum of $Sc_3N@C_{80}$-Cys (I) measured in $CDCl_3$ solution at 298 K.

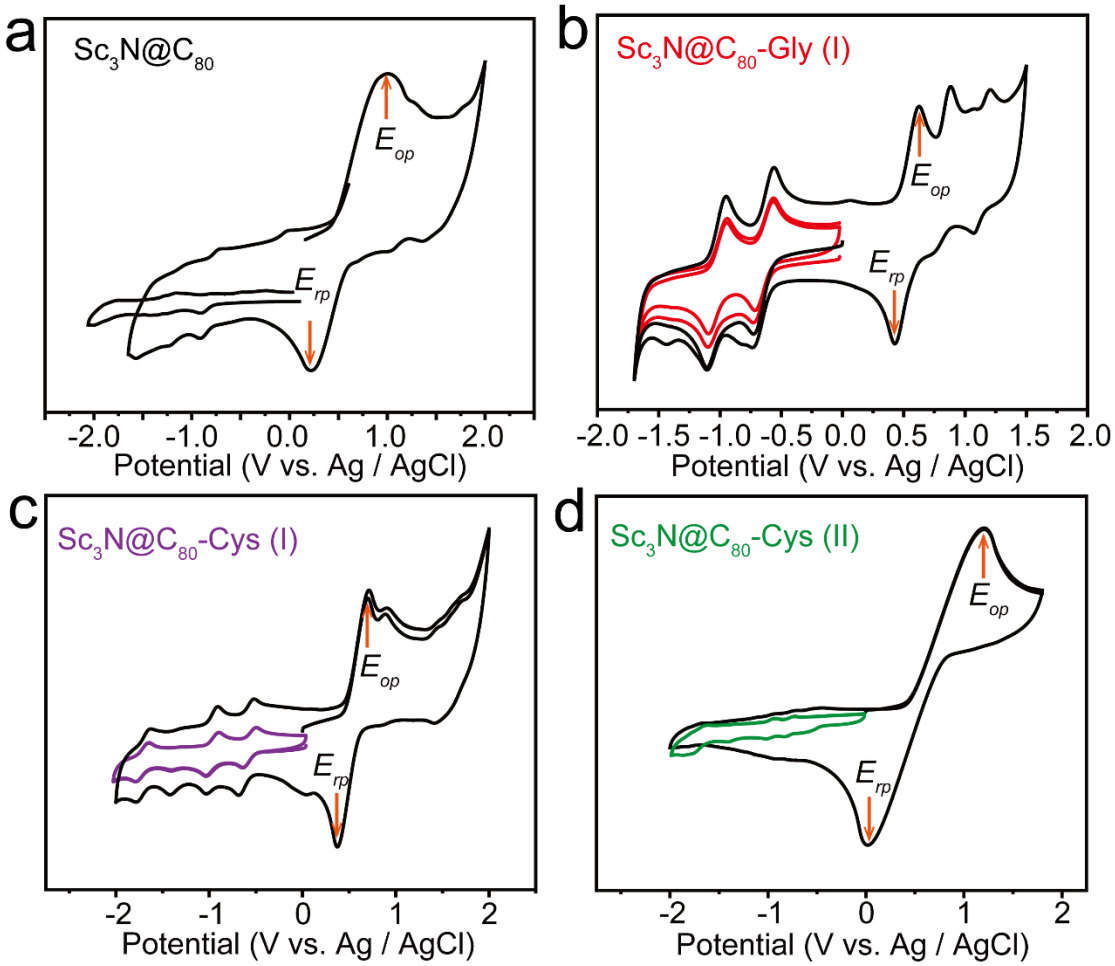


Figure S7. CV curves of $Sc_3N@C_{80}$, $Sc_3N@C_{80}$-Cys (I), $Sc_3N@C_{80}$-Cys (II) and $Sc_3N@C_{80}$-Gly (I) recorded in o-DCB solution containing 0.05 M $TBAPF_6$ with ferrocene as the internal standard, scan rate: 100 mV $s^{-1}$. The potentials were recorded against Ag/AgCl and were calibrated relative to $Fc/Fc^+$ in the main text. The potential against $Fc/Fc^+$ was equal to the half of the sum of oxidation peak potential and redox peak potential using $E\ (Fc/Fc^+) = 1/2\ (E_{op} + E_{rp})$.

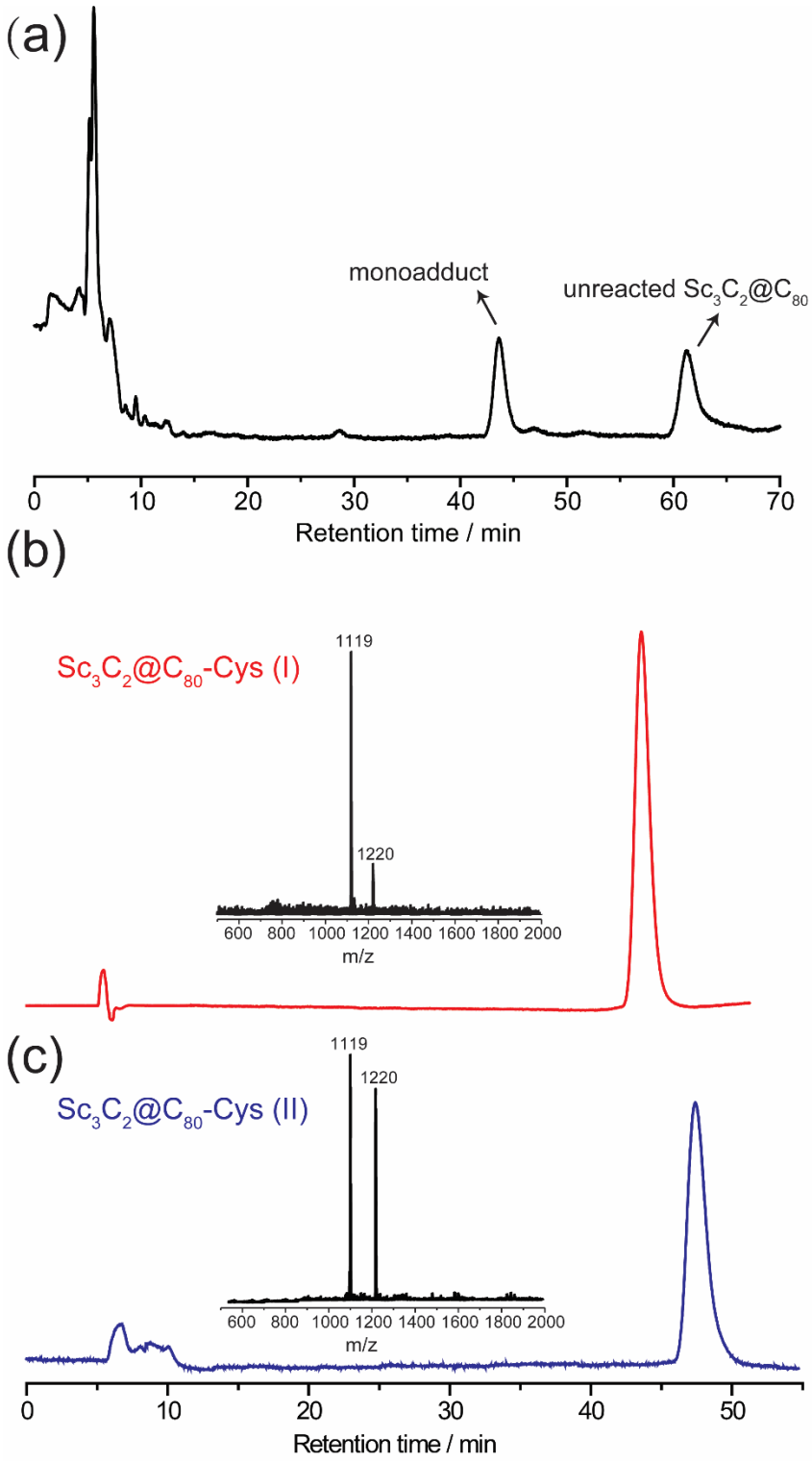


Figure S8. (a) HPLC profile showing the separation process of the crude mixture of the Prato reaction of $Sc_3C_2@C_{80}$. HPLC profile of purified monoadduct of (b) $Sc_3C_2@C_{80}$-Cys (I) and (c) $Sc_3C_2@C_{80}$-Cys (II), inset: the corresponding MALDI-TOF mass spectroscopy. Conditions: Buckyprep column (ø 20×250 mm), 12 mL $min^{-1}$ toluene flow, 310 nm detection wavelength.

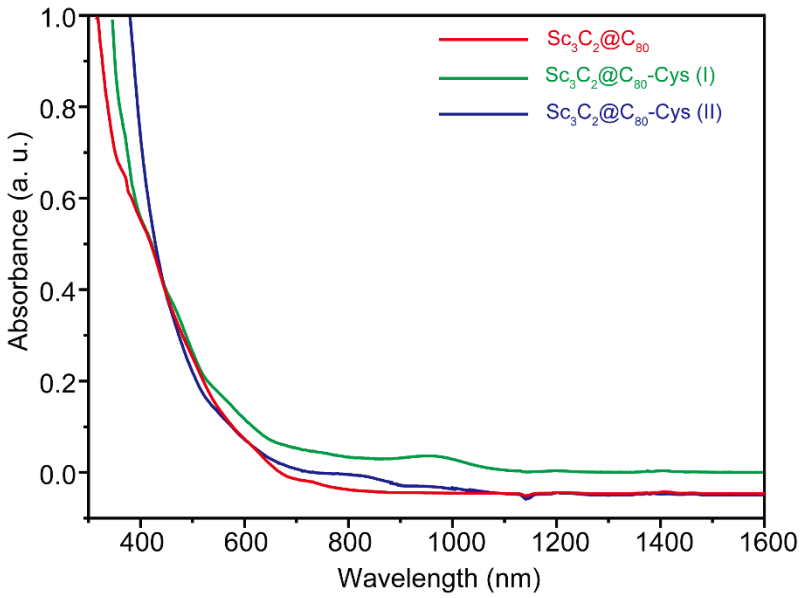


Figure S9. UV-vis-NIR spectra of $Sc_3C_2@C_{80}$, $Sc_3C_2@C_{80}$-Cys (I) and $Sc_3C_2@C_{80}$-Cys (II).